



Providing Choice & Value

Generic CT and MRI Contrast Agents



**FRESENIUS
KABI**

CONTACT REP

AJNR

This information is current as
of July 28, 2025.







**The Inferior Cerebellar Peduncle Sign: A
Novel Imaging Marker for Differentiating
Multiple System Atrophy Cerebellar Type
from Spinocerebellar Ataxia**

Chae Y. Lim, Yujin Seo, Beomseok Sohn, Minjung Seong,
Sung T. Kim, Sungjun Hong, Jinyoung Youn and Eung Y.
Kim

AJNR Am J Neuroradiol published online 14 December
2024

<http://www.ajnr.org/content/early/2025/05/15/ajnr.A8623>

The Inferior Cerebellar Peduncle Sign: A Novel Imaging Marker for Differentiating Multiple System Atrophy Cerebellar Type from Spinocerebellar Ataxia

 Chae Y. Lim,  Yujin Seo, Beomseok Sohn,  Minjung Seong,  Sung T. Kim,  Sungjun Hong, Jinyoung Youn, and  Eung Y. Kim



ABSTRACT

BACKGROUND AND PURPOSE: The hot cross bun (HCB) sign is a hallmark feature of multiple system atrophy with predominant cerebellar ataxia (MSA-C), typically observed in advanced stages of the disease; however, it can also present in other conditions such as spinocerebellar ataxia (SCA), making the differentiation challenging. The middle cerebellar peduncle (MCP) sign may be observed in various medical conditions and in healthy individuals. We hypothesized that the inferior cerebellar peduncle (ICP), known to be affected in MSA-C, may exhibit hyperintensity on FLAIR imaging, potentially aiding in differentiating MSA-C from SCA.

MATERIALS AND METHODS: Medical records of 153 patients with probable MSA-C and 72 genetically confirmed SCAs from a single institution were reviewed retrospectively between January 2012 and June 2023. MRI was performed using 3T scanners. The ICP sign was deemed positive when the bilateral ICP signal intensity exceeded that of the medulla oblongata on axial FLAIR images. MCP and HCB signs were also evaluated. Two independent neuroradiologists evaluated all MRIs, and interobserver agreement was assessed using κ statistics. Univariable and multivariable logistic regression analyses identified predictive features, and diagnostic performance was assessed.

RESULTS: The ICP sign was more prevalent in patients with MSA-C (65%) compared with those with SCA (6.9%; $P < .001$). The HCB and MCP signs were more frequent in patients with MSA-C ($n=110$ and $n=134$) than in those with SCA ($n=19$ and $n=30$; $P < .001$). The ICP sign demonstrated the highest specificity (95%) for predicting MSA-C, with an area under the curve (AUC) = 0.82, respectively. The MCP sign exhibited superior sensitivity (87%) but lower specificity and AUC compared with the ICP sign. Combining the ICP and MCP signs improved the AUC to 0.86. Integrating clinical features (age, sex, and disease duration) with imaging features yielded excellent diagnostic performance, with an AUC = 0.98.

CONCLUSIONS: The ICP sign on FLAIR imaging has high specificity in distinguishing MSA-C from SCA. Integrating clinical and imaging features further enhances diagnostic accuracy, potentially improving the differential diagnosis in clinical settings of cerebellar ataxia.

ABBREVIATIONS: AUC = area under the curve; HCB = hot cross bun; ICP = inferior cerebellar peduncle; ICI = integrated calibration index; IQR = interquartile range; MCP = middle cerebellar peduncle; MDS = Movement Disorder Society; MSA = multiple system atrophy; MSA-C = multiple system atrophy with predominant cerebellar ataxia; SCA = spinocerebellar ataxia

In 2022, the Movement Disorder Society (MDS) revised the 2008 consensus criteria for diagnosing multiple system atrophy (MSA), addressing concerns about the limited diagnostic sensitivity and accuracy of the original criteria, hindering potential treatment opportunities for patients with MSA.¹ The updated criteria introduced additional brain MRI markers for diagnosing clinically established and probable MSA, supplementing the


existing criteria such as atrophy of the putamen and infratentorial structures (pons and middle cerebellar peduncle).² The updates include increased putamen diffusivity on DWI and the hot cross bun (HCB) sign on T2-weighted images, underscoring the expanded role of MRI biomarkers in diagnosis.³⁻⁷ However, this HCB sign typically appears in later stages of MSA and may also occur in other conditions, posing a challenge in distinguishing MSA with predominant cerebellar ataxia (MSA-C) from

Received August 26, 2024; accepted after revision December 6.

From the Department of Radiology and Center for Imaging Science (C.Y.L., Y.S., B.S., M.S., S.T.K., E.Y.K.), Department of Neurology (J.Y.), and Neuroscience Center (J.Y.), Samsung Medical Center, Sungkyunkwan University School of Medicine, Seoul, Republic of Korea; Department of Digital Health (S.H.), Samsung Advanced Institute of Health Sciences and Technology, Sungkyunkwan University, Seoul, Republic of Korea; and Medical AI Research Center (S.H.), Research Institute for Future Medicine, Samsung Medical Center, Seoul, Republic of Korea.

This research was supported by a grant from the Korea Health Technology R&D Project through the Korea Health Industry Development Institute, funded by the Ministry of Health & Welfare, Republic of Korea (grant No: RS-2023-00266288).

Please address correspondence to Eung Yeop Kim, MD, Department of Radiology and Center for Imaging Science, Samsung Medical Center, Sungkyunkwan University School of Medicine, 81 Irwon-ro Gangnam-gu, Seoul 06351, Republic of Korea; e-mail: neuroradkim@gmail.com

 Indicates open access to non-subscribers at www.ajnr.org

 Indicates article with supplemental data.

<http://dx.doi.org/10.3174/ajnr.A8623>

SUMMARY

PREVIOUS LITERATURE: The HCB sign is a characteristic imaging marker of MSA-C, but it can also be present in patients with SCA, limiting its diagnostic specificity. The MCP sign has also shown limited utility due to its presence in various conditions and healthy individuals. Previous pathologic studies have shown involvement of the ICP in MSA-C, but its potential as a diagnostic marker on conventional MRI remains unexplored.

KEY FINDINGS: The ICP sign demonstrated high specificity (95%) and diagnostic performance ($AUC = 0.82$) for differentiating MSA-C from SCA. Integration of clinical features with imaging markers, including the ICP sign, achieved excellent diagnostic accuracy ($AUC = 0.98$).

KNOWLEDGE ADVANCEMENT: We established the ICP sign as a novel, highly specific imaging marker for MSA-C diagnosis using conventional FLAIR imaging. The integration of this sign with other imaging and clinical features provides a comprehensive diagnostic approach for distinguishing MSA-C from SCA.

spinocerebellar ataxia (SCA)—a crucial differential diagnosis in patients with ataxia, given the similarity of their symptoms; however, the grave prognosis of MSA-C is due to progressive autonomic dysfunction and nigrostriatal symptoms associated with α -synucleinopathy.⁸⁻¹⁰

The inferior cerebellar peduncle (ICP) is a bundle of fibers connecting the cerebellum to the medulla oblongata and spinal cord, comprising the restiform and juxtarestiform bodies.¹¹ Previous postmortem studies have identified ICP as the earliest structure damaged by α -synucleinopathy, leading to glial cytoplasmic inclusions and demyelination of affected sites in patients with MSA-C.^{12,13} This observation led researchers to hypothesize that ICP hyperintensity on T2 FLAIR images might reflect these pathologic alterations, potentially serving as a distinct marker for MSA-C. To investigate this hypothesis, we examined its occurrence in our patient cohort and compared it with patients with SCA used as controls. We also assessed the diagnostic performance of ICP hyperintensity and developed a multivariable prediction model incorporating other known brain MRI markers to distinguish MSA-C from SCAs, aiming for more accurate differentiation between these conditions.

MATERIALS AND METHODS

Patient Selection and Baseline Data Collection

This study was approved by the institutional review board of Samsung Medical Center (IRB, 2023-08-001-001). All methods adhered to relevant Standards for Reporting Diagnostic Accuracy Studies (STARD) checklist and regulations, and a waiver of informed consent was granted by the institutional review board (Supplemental Data). Medical records of patients with suspected MSA-C and genetically confirmed SCAs from a single institution were retrospectively reviewed. Between January 2012 to June 2023, one hundred seventy-nine patients with MSA-C were initially identified; eventually, 153 patients were included on the basis of the second consensus diagnostic criteria of MSA-C.^{1,14} Patients with a static course, lacking autonomic failure as described in the criteria, or presenting with other explicable causes of cerebellar ataxia were excluded. Furthermore, in those who manifested initial symptoms before 50 years of age, SCA

panel tests were conducted to exclude the possibility of autosomal dominant cerebellar ataxia.

Regarding SCA, 80 patients with positive genetic test findings visited our center in the same period. Patients in the MSA-C and the SCA group were included if their MRI scans were obtained at the onset of symptoms. Patients whose MRI findings were unavailable or unsuitable for assessment were excluded, resulting in 72 patients with SCA being included (Fig 1). Baseline characteristics such as sex, age of onset, and disease duration at the time of the MRI acquisition were obtained. Disease duration was calculated from the symptom onset, on the basis of medical records, indicating any of the following features: gait disturbance due to imbalance or slowness; dysarthria; hand incoordination; postural dizziness, or syncope; urinary incontinence or retention; erectile dysfunction; dizziness unexplained by otologic problems or postural change; decreased visual acuity; parkinsonism; and dystonia.^{15,16}

MRI Acquisition and Analysis

MRI was performed using 3T scanners (Achieva, Ingenia, Ingenia CX, Philips Healthcare; and Genesis, Signa, GE Healthcare) with a standard 16-to-64 channel head coil. Image acquisitions were

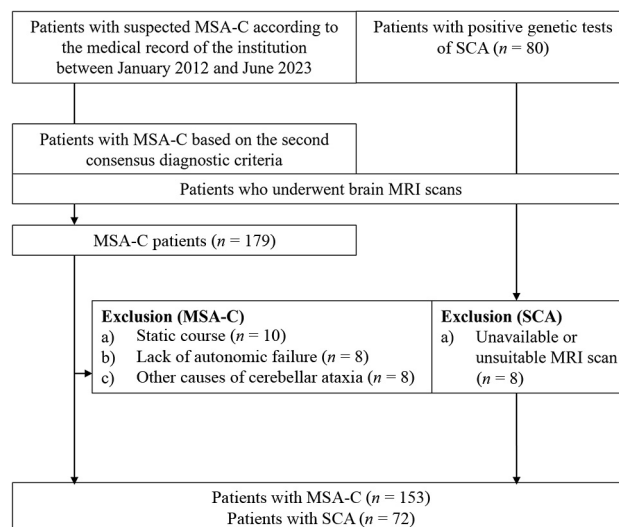


FIG 1. Study flow chart.

conducted as follows: 1) axial T2-weighted images: TR, 3000–4083 ms; TE, 80–99 ms; echo-train length = 15–16 ms; and 5.0-mm thickness); 2) axial T2 FLAIR: TR, 9000–11,000 ms; TE, 103.5–125 ms; echo-train length = 0–38 ms; and 5.0-mm thickness); 3) sagittal T1-weighted images: TR, 9.9–416 ms; TE, 4.6–9 ms; echo-train length = 16–240 ms; and 5.0-mm thickness).

The ICP sign was considered positive when the signal intensity of the bilateral ICPs was higher than that of the medulla oblongata on axial FLAIR images (Fig 2). The MCP sign was marked as present or absent on the basis of MCP hyperintensity on T2-weighted and FLAIR images (Fig 3).^{17–19} The HCB sign was considered present when both horizontal and vertical lines

were observed in the pons,³ whereas the vertical line sign was considered present when observed either as an isolated vertical line or as the vertical component of cruciform hyperintensity in the pons.²⁰ Cerebellar atrophies were visually evaluated regarding the vermis and hemispheres.^{21,22} Two independent neuroradiology specialists (B.S. and C.Y.L.) blinded to clinical information evaluated all MRIs. In cases of discrepancy between the 2 neuroradiologists, the analysis was decided by a consensus between them. The presence of MCP, ICP, HCB, and vertical line signs was assessed on axial FLAIR images. Cerebellar atrophies were assessed on sagittal T1-weighted images.

Statistical Analysis: Development and Assessment of the Prediction Model

We explored the complete data set to identify and select variables for predicting MSA-C. Clinical and imaging features were summarized by median with range or frequency with percentage, depending on variable types and compared between the MSA-C and SCA groups using the Student *t*, Mann-Whitney *U*, χ^2 , and Fisher exact tests as appropriate. Interobserver agreement was measured by κ statistics. Using features with high predictive values in the exploratory univariable analysis, we underwent multivariable logistic regression, with a stepwise variable selection using the Akaike information criterion. For model development and internal validation, we

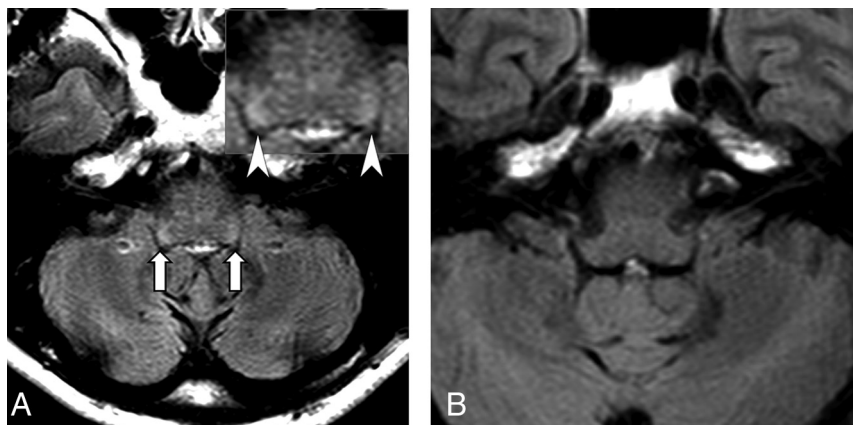


FIG 2. Representative cases of positive/negative ICP signs. *A*, A 45-year-old woman presented with cerebellar ataxia. A FLAIR image reveals increased signal intensity in the bilateral inferior cerebellar peduncles (arrows; arrowheads in an inset) compared with the medulla. The patient was diagnosed with MSA-C. *B*, In the T2 FLAIR image of a 48-year-old man diagnosed with spinocerebellar ataxia, no ICP sign is seen.

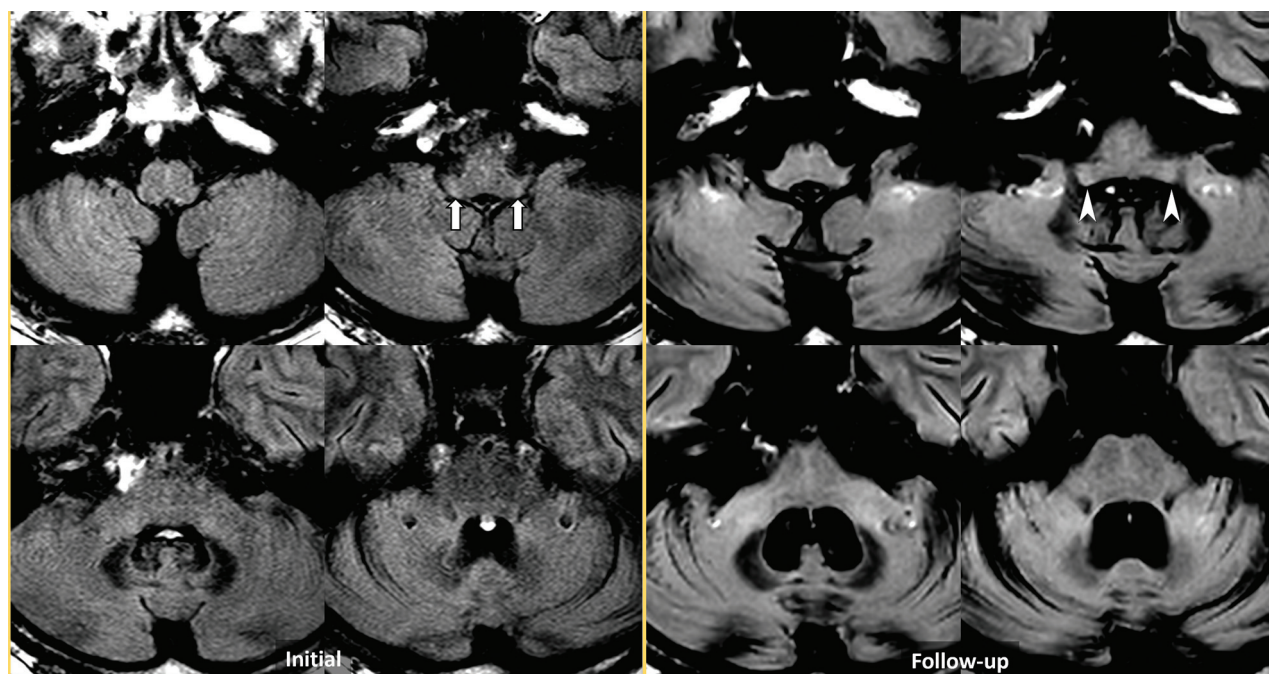


FIG 3. FLAIR imaging in a 53-year-old man who presented with cerebellar ataxia. The initial imaging (left) showed high signal intensity in both inferior cerebellar peduncles (arrows), defined as the ICP sign. However, the MCP sign was not evident. On 15-month follow-up MRI (right), the ICP sign was again noted (arrowheads), and both the HCB and MCP signs appeared. The patient was diagnosed as having MSA-C.

Table 1: Demographic characteristics and frequency analysis of MRI findings^a

| Variables | Total (n = 225) | MSA-C (n = 153) | SCA (n = 72) | P Values |
|------------------------------------|-----------------------|--------------------|-----------------|-------------|
| Clinical features | | | | |
| Age ^a | 59 (53–65) | 60 (56–67) | 53 (44–61) | <.001 |
| Disease duration (yr) ^a | 3 (1–5) | 2 (1–3.3) | 5 (2–11) | <.001 |
| Sex | | | | |
| Male | 124 (55) ^b | 79 (52) | 45 (63) | .204 |
| Female | 101 (45) | 74 (48) | 27 (38) | |
| Imaging features | | | | |
| Scanner | | | | .053 |
| A | 182 (81) | 119 (78) | 63 (88) | |
| B | 6 (2.7) | 4 (2.6) | 2 (2.8) | |
| C | 36 (16) | 30 (20) | 6 (8.3) | |
| D | 1 (0.4) | 0 (0.0) | 1 (1.4) | |
| ICP sign | 105 (47) | 100 (65) | 5 (6.9) | <.001 |
| HCB sign | 129 (57) | 110 (72) | 19 (26) | <.001 |
| MCP sign | 164 (73) | 134 (88) | 30 (42) | <.001 |
| Cerebellar atrophy | 191 (85) | 135 (88) | 56 (78) | .065 |
| Vertical line | 180 (80) | 132 (86) | 48 (67) | .011 |

^a Data are presented as median (1st quartile, 3rd quartile).^b Percentages in parenthesis.**Table 2: Univariable and multivariable logistic regression analyses for predicting the MSA with predominant cerebellar ataxia group**

| Variables | Univariable Analysis | | | Multivariable Analysis | | |
|------------------------------|----------------------|-----------|---------|------------------------|-----------|---------|
| | OR | 95% CI | P Value | OR | 95% CI | P Value |
| Age | 1.10 | 1.07–1.14 | <.001 | 1.16 | 1.09–1.28 | <.001 |
| Disease duration (yr) | 0.77 | 0.70–0.85 | <.001 | 0.63 | 0.53–0.75 | <.001 |
| Sex (male) | 1.58 | 0.89–2.81 | .117 | | | |
| Scanner (A) ^a | 2.02 | 0.91–4.47 | .084 | | | |
| ICP sign (absence) | 25.7 | 9.78–67.9 | <.001 | 32.7 | 5.74–186 | <.001 |
| HCB sign (absence) | 7.31 | 3.88–13.8 | <.001 | | | |
| MCP sign (absence) | 10.4 | 5.28–20.6 | <.001 | 16.8 | 5.08–55.8 | <.001 |
| Cerebellar atrophy (absence) | 2.27 | 1.07–4.81 | .032 | | | |
| Vertical line (absence) | 3.30 | 1.67–6.54 | .001 | | | |

^a Scanner A (the most frequently used scanner type) is the reference, with the OR calculated for other scanner types combined. The reference category for each variable is presented in parentheses.

used stratified random sampling to divide the data set into training (70%) and test (30%) cohorts, maintaining balanced proportions of MSA-C and SCA cases in each cohort.

Diagnostic outcomes were evaluated using the area under the receiver operating curves (AUC) with various other measures, including sensitivity and specificity. Calibration was assessed by drawing calibration plots using a locally-weighted scatterplot smoothing curve to illustrate the relationship between the predicted and observed probability of MSA-C. All statistical procedures were performed using R Software (Version 4.1.0; <http://www.r-project.org/>).

RESULTS

Patient Characteristics

Among the 225 patients in our study, 153 (68%) were diagnosed with MSA-C on the basis of the MDS criteria for the diagnosis of MSA, while 72 (32%) were diagnosed with SCA. The SCA group included 7 subtypes: SCA1 (4 patients), SCA2 (21 patients), SCA3 (18 patients), SCA5 (11 patients), SCA6 (8 patients), SCA7 (5 patients), and SCA36 (5 patients). The cohort included 124

men (55%) with a median age of 59 years, ranging from 19 to 81 years of age (Table 1).

The median age at diagnosis differed between the MSA-C and SCA groups, with patients with MSA-C being older (median age, 60 years; interquartile range [IQR], 56–67 years) compared with patients with SCA (median age, 53 years; IQR, 44–61 years; $P < .001$). Similarly, disease duration differed; patients with MSA-C had a shorter median disease duration (2 years; IQR, 1–3.3 years) compared with those with SCA (5 years; IQR, 2–11 years; $P < .001$).

In terms of image acquisition, scanner A was the most frequently used in both groups (78% in MSA-C and 88% in SCA), and the Fisher exact test showed no significant difference in scanner distribution between the 2 groups ($P = .053$). The distribution of sexes across the groups demonstrated no difference ($P = .204$). These patients were divided into training and test cohorts, with the baseline characteristics summarized in Supplemental Data. Both cohorts were balanced for the MSA-C rate and were not statistically different (all, $P > .05$).

Imaging Analysis

Imaging findings of the participants are summarized in Table 1. The presence of the ICP sign was more common in

patients with MSA-C (65%, $n = 100$) compared with those with SCA (6.9%, $n = 5$; $P < .001$). All 5 patients with SCA with the ICP sign were the SCA2 subtype. The HCB, MCP, and vertical line signs were also more prevalent in patients with MSA-C, occurring in 110 (72%), 134 (88%), and 132 (86%) of cases, respectively, compared with 19 (26%), 30 (42%), and 48 (67%) in patients with SCA ($P < .001$, $P < .001$, and $P = .011$). Cerebellar atrophy was observed in patients with MSA-C (88%, $n = 135$) and those with SCA (78%, $n = 56$; $P = .065$). Interobserver agreement of those findings is summarized in the Supplemental Data. Except for cerebellar atrophy, other imaging findings exhibited substantial interobserver agreement.

Multiple Logistic Regression Analysis for Predicting the MSA-C

In the multivariable logistic regression analysis, age remained a strong predictor (OR, 1.16; 95% CI, 1.09–1.28; $P < .001$). Disease duration demonstrated an inverse relationship in the multivariable analysis (OR, 0.63; 95% CI, 0.53–0.75; $P < .001$). Among imaging features, the ICP and MCP signs were significant predictors in the multivariable analysis (OR, 32.7; 95% CI, 5.74–186;

Table 3: Diagnostic performance of imaging and clinical features for predicting the MSA with the predominant cerebellar ataxia group

| Parameters | Sensitivity ^a | Specificity ^a | F1 Score | AUC ^b | P Value ^c |
|-------------------------------|--------------------------|--------------------------|----------|------------------|----------------------|
| ICP | 0.69 [31/45] | 0.95 [20/21] | 0.73 | 0.82 (0.74–0.90) | – |
| MCP | 0.87 [39/45] | 0.48 [10/21] | 0.69 | 0.67 (0.55–0.79) | .029 |
| HCB | 0.69 [31/45] | 0.71 [15/21] | 0.64 | 0.70 (0.58,0.82) | .052 |
| ICP + MCP | 0.62 [28/45] | 0.95 [20/21] | 0.70 | 0.86 (0.78–0.98) | .114 |
| Integrated model ^d | 0.87 [39/45] | 1.00 [21/21] | 0.88 | 0.98 (0.96–1.00) | <.001 |

Note:—The en dash indicates not applicable.

^aData in brackets indicate the number of corresponding patients for each of the metric.

^bData in parentheses are 95% CIs with the DeLong test.

^cP values of AUCs compared with ICP as a reference.

^dIntegrated model includes the ICP, MCP sign, age, and disease duration as variables.

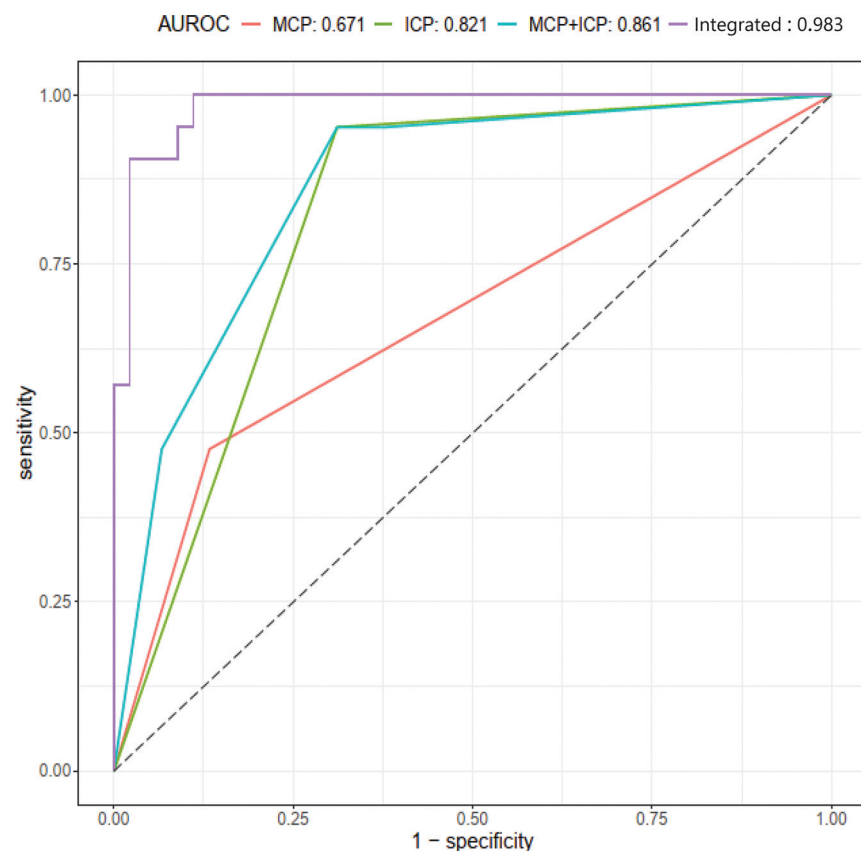


FIG 4. Receiver operating curves of ICP, MCP, combined ICP and MCP signs and the integrated clinicoradiologic model for predicting MSA-C. The AUCs of the ICP sign, MCP sign, and combined ICP and MCP signs are 0.82, 0.67, and 0.86, respectively. The integrated model shows the highest diagnostic performance (AUC = 0.98, 95% CI, 0.96–1.00).

$P < .001$; OR, 16.8; 95% CI, 5.08–55.8; $P < .001$), highlighting its importance (Table 2).

Diagnostic Performance of Imaging and Clinical Features

The diagnostic performance for 2 imaging features (the ICP and MCP signs) and their combinations, the HCB sign and the integrated imaging and clinical feature (age, sex, and disease duration) model are summarized in Table 3 and Fig 4. Among them, the ICP sign had the highest specificity (95%) and AUC (0.82; 95% CI, 0.74–0.90) for predicting MSA-C compared with other imaging biomarkers. The MCP sign exhibited the best sensitivity (87%); however, its specificity was <50%, with its AUC being

lower than that of the ICP sign (0.67; 95% CI, 0.55–0.79; $P = .029$). The HCB sign demonstrated moderate sensitivity, specificity, and AUC (0.70; 95% CI, 0.58–0.82). When we combined the ICP and MCP signs, which were independently predictive of MSA-C in the multivariable analysis, its AUC improved to 0.86 (95% CI, 0.78–0.98), though not different from ICP alone ($P = .114$). When we integrated clinical and all evaluated imaging features, it demonstrated excellent diagnostic performance with a sensitivity of 87% and a specificity of 100%. The F1 score was 0.88, and the AUC was notably high at 0.98 (95% CI, 0.96–1.00), outperforming the ICP sign alone ($P < .001$). In subgroup analysis comparing patients with early (<3 years) and late (≥ 3 years) disease duration, the AUC of the ICP sign did not significantly differ between those 2 groups (0.83 and 0.77, respectively, $P = .187$). Notably, in the early disease phase, combining the ICP and MCP signs significantly improved diagnostic performance (AUC = 0.92) compared with either ICP sign alone ($P < .001$) or the MCP sign alone ($P = .005$), achieving both high sensitivity (94%) and specificity (74%, Supplemental Data).

We further assessed the reliability of these imaging predictors and models using the calibration plots and measures (Fig 5). The ICP model showed reliable calibration (intercept = 0.12, slope = 1.25), closely approximating the reference line with a small integrated calibration index (ICI) of 0.03. The MCP model demonstrated systematic underestimation (intercept = –0.13) with extreme predictions (slope = 0.71) and an increased ICI of 0.61. The combined model (ICP and

MCP signs) showed systematic overestimation (intercept = 0.30) with slightly moderate predictions (slope = 1.17) and ICI of 0.62. While the integrated imaging and clinical model maintained near-optimal systematic calibration (intercept = 0.02) and the lowest ICI (0.03), its slope (1.74) notably deviated from the reference line, indicating too moderate predictions.^{23,24} The ICP model demonstrates good overall performance with balanced calibration metrics.

DISCUSSION

Our study revealed that approximately two-thirds of patients with MSA-C exhibited the ICP sign, a rate comparable with that

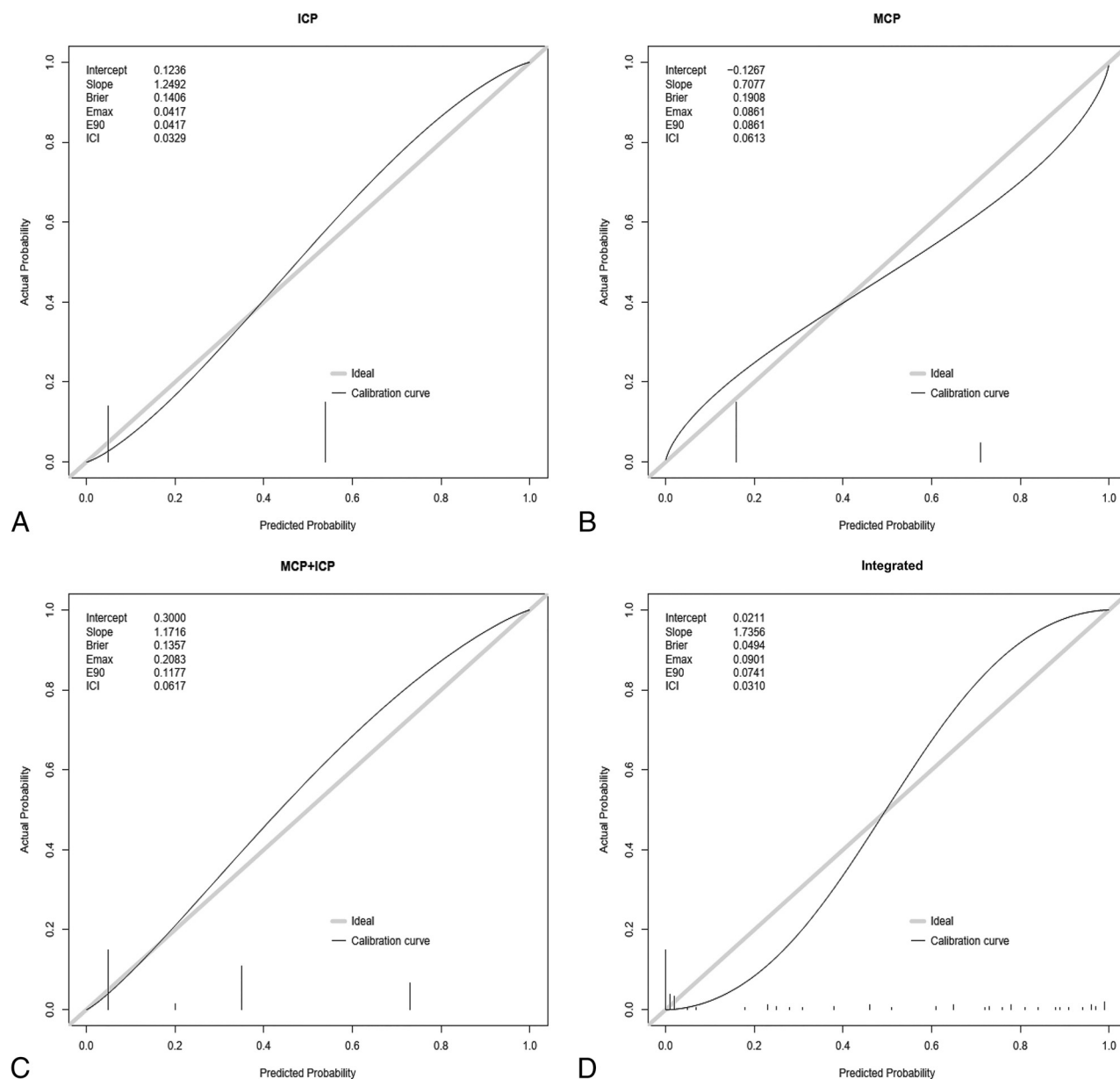


FIG 5. Calibration plots with ICIs of the ICP, MCP, combined ICP and MCP hyperintensity signs, and the integrated clinicoradiologic model for predicting MSA-C. Calibration plots comparing the ICP sign (intercept = 0.12, slope = 1.25, ICI = 0.03), MCP sign (intercept = -0.13, slope = 0.71, ICI = 0.61), combined signs (intercept = 0.30, slope = 1.17, ICI = 0.62), and integrated model (intercept = 0.02, slope = 1.74, ICI = 0.03). The ICP sign demonstrates reliable calibration overall. Bars in the calibration plot denote observed outcome frequencies within each bin, reflecting the calibration level of the prediction model. The diagonal line indicates perfect calibration. Brier indicates the Brier score (average squared difference in predicted and actual probabilities); Emax/E90/ICI, the maximum/90th quantile/weighted average of absolute difference in predicted and actual calibrated probabilities.

of the HCB sign. While the MCP hyperintensity sign was more common than the ICP sign, it was also observed in >40% of patients with SCA. Previous studies have documented the MCP hyperintensity sign in varying conditions, including healthy individuals, and our research corroborates its presence in a notable proportion of patients with SCA.^{25,26}

More than one-quarter of patients with SCA had the HCB sign in our study. This finding is consistent with several reports showcasing the presence of the HCB sign in patients with SCA.^{8,27-29} The vertical line sign (also known as the vertical pontine hyperintensity) typically marks the initial stage of the HCB

sign and progresses to a complete cruciform hyperintensity in advanced MSA.²⁰ While Sugiyama et al³⁰ found no significant group differences in the vertical line sign between patients with MSA-C and SCA3, our larger cohort demonstrated that it could differentiate MSA-C from SCAs. This result may be explained by the greater statistical power of our study.

The diagnostic performance for the ICP sign was the highest among the signs studied, notably for its specificity, which exceeded 95% in our test cohort. This specificity surpassed that of the HCB sign, an imaging biomarker currently recognized in the MDS consensus criteria for diagnosing MSA-C.¹ The high

specificity of the ICP sign is particularly valuable, given the diagnostic challenges of SCA, which presents similar clinical symptoms and nonspecific imaging findings.^{28,31,32} Furthermore, incorporating age and disease duration into our model increased the test AUC to 0.98, marking the first attempt, to our knowledge, to establish an integrated clinoradiologic model.

Studies have demonstrated that 3D FLAIR sequences enable more detailed visualization of brainstem structures³³ and provide superior lesion detection compared with conventional 2D-FLAIR in various white matter pathologies.^{34,35} Future studies using 3D FLAIR imaging techniques might further enhance the diagnostic accuracy of ICP assessment in differentiating MSA-C from SCA.

Pathologic studies in MSA have revealed pallor or loss of myelin staining in white matter tracts, where glial cytoplasmic inclusions—the diagnostic hallmark of MSA—are frequently observed, particularly in intrafascicular oligodendrocytes.³⁶ Building on these pathologic findings, a DTI study by Shiga et al³⁷ identified decreased fractional anisotropy of the ICP in one-half of the patients with MSA, encompassing both parkinsonian and cerebellar variants, compared with age-matched controls. Subsequently, Oishi et al,³⁸ focusing specifically on patients with MSA-C, reported reduced fractional anisotropy values in the ICP, even during the early stages of the disease. Furthermore, comparative DTI studies between MSA-C and SCA1 have demonstrated significant differences in fractional anisotropy values of ICP at the group level.³⁹ In line with these previous DTI studies, we observed similar ICP abnormalities using T2 FLAIR imaging and showed a high diagnostic value at the individual level.

Because clinically differentiating MSA-C and SCA is challenging, especially in the early stage, imaging markers with reliable early diagnostic value are particularly important. Kim et al⁹ reported the increased differential value of conventional MRI signs (HCB and MCP hyperintensity) during early disease stages when comparing MSA-C and SCAs. Similarly, our subgroup analysis demonstrated that the ICP sign maintains robust diagnostic performance in both early (<3 years; AUC = 0.83) and late disease-duration groups (≥ 3 years; AUC = 0.77), with notably high specificity (100%) in the early group.

In our study, the ICP sign was observed in 5 of 21 patients with genetically confirmed SCA2. Notably, these cases, which represent all the false-positives in our cohort, tended to have a longer disease duration and more prominent brainstem atrophy. Previous studies have described characteristic brainstem involvement in SCA2,⁴⁰ with postmortem studies by Estrada et al⁴¹ showing involvement of the inferior olivary neurons and olivocerebellar fibers and Yoshii et al⁴² reporting inferior olive hyperintensity on MRI. While our study establishes the ICP sign as a useful marker for differentiating MSA-C from SCA, these observations suggest careful consideration may be needed when applying it to cases of advanced SCA2.

Our study has limitations. First, it did not encompass the full spectrum of diseases in progressive cerebellar ataxia. Given the rarity of conditions such as sporadic adult-onset ataxia of unknown etiology and idiopathic late-onset cerebellar ataxia,⁴³ which are diagnoses of exclusion, these were not included in our cohort. Our primary aim was to differentiate MSA-C and SCA, the 2 most prevalent and important causes of this condition in

adults.⁴³ Second, the retrospective nature of our study may introduce biases, including selection bias and reliance on the quality of historical data. Additionally, the age distribution of patients with MSA-C and those with SCA differed in our cohort. We did not match the ages of these groups, because matching could not fully mitigate this limitation or simulate the conditions of a randomized controlled trial. Moreover, matching would have reduced the number of patients, thereby diminishing the statistical power of our study. Third, we cannot fully elucidate the biologic background of the high specificity of the ICP sign for differentiating MSA-C from SCA. Ataxia-causing lesions in SCA invariably affect the “cerebellar module,” which is defined as the reciprocal circuitry among the cerebellar cortex, dentate nuclei, and inferior olivary nuclei. An overlap of the affected sites seen in both MSA-C and SCA implies that further histopathologic studies are needed to explain the high specificity of the ICP sign in MSA, because it cannot be solely attributed to the known gliosis or cell loss in the cerebellar cortex and inferior olivary nuclei.^{12,44} Last, the analysis of imaging findings was qualitative, relying on the visual assessment of radiologic signs. This approach is susceptible to interobserver variability and may lack the precision of quantitative imaging analyses, potentially affecting the reproducibility and objectivity of our results.

Despite these limitations, our research offers potential benefits for patients with late-onset progressive ataxia in movement disorder clinics, offering insights that may enhance diagnostic accuracy and thereby inform potential treatment strategies.

CONCLUSIONS

We identified a new complementary imaging biomarker for MSA-C—hyperintensity of the ICP on FLAIR imaging—that reflects the pathologic alterations in MSA-C. We demonstrated its diagnostic utility both as a stand-alone marker and in combination with other imaging biomarkers and clinical features for differentiating MSA-C from SCA.

Disclosure forms provided by the authors are available with the full text and PDF of this article at www.ajnr.org.

REFERENCES

1. Wenning GK, Stankovic I, Vignatelli L, et al. **The Movement Disorder Society Criteria for the Diagnosis of Multiple System Atrophy.** *Mov Disord* 2022;37:1131–48 [CrossRef Medline](#)
2. Schrag A, Good CD, Miskiel K, et al. **Differentiation of atypical parkinsonian syndromes with routine MRI.** *Neurology* 2000;54:697–702 [CrossRef Medline](#)
3. Schrag A, Kingsley D, Phatouros C, et al. **Clinical usefulness of magnetic resonance imaging in multiple system atrophy.** *J Neurol Neurosurg Psychiatry* 1998;65:65–71 [CrossRef Medline](#)
4. Baudrexel S, Seifried C, Penndorf B, et al. **The value of putaminal diffusion imaging versus 18-fluorodeoxyglucose positron emission tomography for the differential diagnosis of the Parkinson variant of multiple system atrophy.** *Mov Disord* 2014;29:380–87 [CrossRef Medline](#)
5. Krismer F, Beliveau V, Seppi K, et al. **Automated analysis of diffusion-weighted magnetic resonance imaging for the differential diagnosis of multiple system atrophy from Parkinson's disease.** *Mov Disord* 2021;36:241–45 [CrossRef Medline](#)

6. Kim HJ, Jeon B, Fung VS. Role of magnetic resonance imaging in the diagnosis of multiple system atrophy. *Mov Disord Clin Pract* 2017;4:12–20 [CrossRef Medline](#)
7. Bajaj S, Krismer F, Palma JA, et al. Diffusion-weighted MRI distinguishes Parkinson disease from the parkinsonian variant of multiple system atrophy: a systematic review and meta-analysis. *PLoS One* 2017;12:e0189897 [CrossRef Medline](#)
8. Burk K, Skalej M, Dichgans J. Pontine MRI hyperintensities (“the cross sign”) are not pathognomonic for multiple system atrophy (MSA). *Mov Disord* 2001;16:535–35 [CrossRef](#)
9. Kim M, Ahn JH, Cho Y, et al. Differential value of brain magnetic resonance imaging in multiple system atrophy cerebellar phenotype and spinocerebellar ataxias. *Sci Rep* 2019;9:17329 [CrossRef Medline](#)
10. Nishida K, Futamura N. Hot cross bun sign in bilateral middle cerebellar peduncle infarction. *Stroke* 2023;54:e163–64 [CrossRef Medline](#)
11. Kadri PAS. The Brainstem and the Cerebellum. In: *The Cartographic Atlas of the Brain*: Springer; 2023:293–451
12. Wenning GK, Tison F, Ben Shlomo Y, et al. Multiple system atrophy: a review of 203 pathologically proven cases. *Mov Disord* 1997;12:133–47 [CrossRef Medline](#)
13. Brettschneider J, Irwin DJ, Boluda S, et al. Progression of alpha-synuclein pathology in multiple system atrophy of the cerebellar type. *Neuropathol Appl Neurobiol* 2017;43:315–29 [CrossRef Medline](#)
14. Gilman S, Wenning GK, Low PA, et al. Second consensus statement on the diagnosis of multiple system atrophy. *Neurology* 2008;71:670–76 [CrossRef Medline](#)
15. Luo L, Wang J, Lo RY, et al. The initial symptom and motor progression in spinocerebellar ataxias. *Cerebellum* 2017;16:615–22 [CrossRef Medline](#)
16. McKay JH, Cheshire WP. First symptoms in multiple system atrophy. *Clin Auton Res* 2018;28:215–21 [CrossRef Medline](#)
17. Savoiardo M, Strada L, Girotti F, et al. Olivopontocerebellar atrophy: MR diagnosis and relationship to multisystem atrophy. *Radiology* 1990;174:693–96 [CrossRef Medline](#)
18. Schulz JB, Klockgether T, Petersen D, et al. Multiple system atrophy: natural history, MRI morphology, and dopamine receptor imaging with 123IBZM-SPECT. *J Neurol Neurosurg Psychiatry* 1994;57:1047–56 [CrossRef Medline](#)
19. Carre G, Dietemann JL, Gebus O, et al. Brain MRI of multiple system atrophy of cerebellar type: a prospective study with implications for diagnosis criteria. *J Neurol* 2020;267:1269–77 [CrossRef Medline](#)
20. Horimoto Y, Aiba I, Yasuda T, et al. Longitudinal MRI study of multiple system atrophy - when do the findings appear, and what is the course? *J Neurol* 2002;249:847–54 [CrossRef Medline](#)
21. Nabatame H, Fukuyama H, Akiguchi I, et al. Spinocerebellar degeneration: qualitative and quantitative MR analysis of atrophy. *J Comput Assist Tomogr* 1988;12:298–303 [CrossRef Medline](#)
22. Klockgether T, Schroth G, Diener HC, et al. Idiopathic cerebellar ataxia of late onset: natural history and MRI morphology. *J Neurol Neurosurg Psychiatry* 1990;53:297–305 [CrossRef Medline](#)
23. Van Calster B, Nieboer D, Vergouw Y, et al. A calibration hierarchy for risk models was defined: from utopia to empirical data. *J Clin Epidemiol* 2016;74:167–76 [CrossRef Medline](#)
24. Van Calster B, McLernon DJ, van Smeden M, et al; Topic Group ‘Evaluating diagnostic tests and prediction models’ of the STRATOS initiative. Calibration: the Achilles heel of predictive analytics. *BMC Med* 2019;17:230 [CrossRef Medline](#)
25. Okamoto K, Tokiguchi S, Furusawa T, et al. MR features of diseases involving bilateral middle cerebellar peduncles. *AJNR Am J Neuroradiol* 2003;24:1946–54 [Medline](#)
26. Ngai S, Tang YM, Du L, et al. Hyperintensity of the middle cerebellar peduncles on fluid-attenuated inversion recovery imaging: variation with age and implications for the diagnosis of multiple system atrophy. *AJNR Am J Neuroradiol* 2006;27:2146–48 [Medline](#)
27. Lee YC, Liu CS, Wu HM, et al. The ‘hot cross bun’ sign in the patients with spinocerebellar ataxia. *Eur J Neurol* 2009;16:513–16 [CrossRef Medline](#)
28. Meira AT, Arruda WO, Ono SE, et al. Neuroradiological findings in the spinocerebellar ataxias. *Tremor Other Hyperkinet Mov (N Y)* 2019;9 [CrossRef Medline](#)
29. Way C, Pettersson D, Hiller A. The ‘hot cross bun’ sign is not always multiple system atrophy: etiologies of 11 cases. *J Mov Disord* 2019;12:27–30 [CrossRef Medline](#)
30. Sugiyama A, Yokota H, Yamanaka Y, et al. Vertical pons hyperintensity and hot cross bun sign in cerebellar-type multiple system atrophy and spinocerebellar ataxia type 3. *BMC Neurol* 2020;20:157 [CrossRef Medline](#)
31. Furtado S, Payami H, Lockhart PJ, et al. Profile of families with parkinsonism-predominant spinocerebellar ataxia type 2 (SCA2). *Mov Disord* 2004;19:622–29 [CrossRef Medline](#)
32. De Joanna G, De Rosa A, Salvatore E, et al. Autonomic nervous system abnormalities in spinocerebellar ataxia type 2: a cardiovascular neurophysiologic study. *J Neurol Sci* 2008;275:60–63 [CrossRef Medline](#)
33. Kitajima M, Hirai T, Shigematsu Y, et al. Comparison of 3D FLAIR, 2D FLAIR, and 2D T2-weighted MR imaging of brainstem anatomy. *AJNR Am J Neuroradiol* 2012;33:922–27 [CrossRef Medline](#)
34. Tawfik AI, Kamr WH. Diagnostic value of 3D-FLAIR magnetic resonance sequence in detection of white matter brain lesions in multiple sclerosis. *Egypt J Radiol Nucl Med* 2020;51:1–9 [CrossRef](#)
35. de Graaf WL, Zwanenburg JJ, Visser F, et al. Lesion detection at seven Tesla in multiple sclerosis using magnetisation prepared 3D-FLAIR and 3D-DIR. *Eur Radiol* 2012;22:221–31 [CrossRef Medline](#)
36. Papp MI, Kahn JE, Lantos PL. Glial cytoplasmic inclusions in the CNS of patients with multiple system atrophy (striatonigral degeneration, olivopontocerebellar atrophy and Shy-Drager syndrome). *J Neurol Sci* 1989;94:79–100 [CrossRef Medline](#)
37. Shiga K, Yamada K, Yoshikawa K, et al. Local tissue anisotropy decreases in cerebellopetal fibers and pyramidal tract in multiple system atrophy. *J Neurol* 2005;252:589–96 [CrossRef Medline](#)
38. Oishi K, Konishi J, Mori S, et al. Reduced fractional anisotropy in early-stage cerebellar variant of multiple system atrophy. *J Neuroimaging* 2009;19:127–31 [CrossRef Medline](#)
39. Prakash N, Hageman N, Hua X, et al. Patterns of fractional anisotropy changes in white matter of cerebellar peduncles distinguish spinocerebellar ataxia-1 from multiple system atrophy and other ataxia syndromes. *Neuroimage* 2009;47(Suppl 2):T72–81 [CrossRef Medline](#)
40. Klockgether T, Skalej M, Wedekind D, et al. Autosomal dominant cerebellar ataxia type I. MRI-based volumetry of posterior fossa structures and basal ganglia in spinocerebellar ataxia types 1, 2 and 3. *Brain* 1998;121(Pt 9):1687–93 [CrossRef Medline](#)
41. Estrada R, Galarraga J, Orozco G, et al. Spinocerebellar ataxia 2 (SCA2): morphometric analyses in 11 autopsies. *Acta Neuropathol* 1999;97:306–10 [CrossRef Medline](#)
42. Yoshii F, Tomiyasu H, Watanabe R, et al. MRI signal abnormalities of the inferior olivary nuclei in spinocerebellar ataxia type 2. *Case Rep Neurol* 2017;9:267–71 [CrossRef Medline](#)
43. Kim JS, Kwon S, Ki CS, et al. The etiologies of chronic progressive cerebellar ataxia in a Korean population. *J Clin Neurol* 2018;14:374–80 [CrossRef Medline](#)
44. Koeppen AH. The pathogenesis of spinocerebellar ataxia. *Cerebellum* 2005;4:62–73 [CrossRef Medline](#)